

Polar flock with bond disorder

Jay Prakash Singh^{1,*}, Sudipta Pattanayak^{2,†} and Shradha Mishra^{1‡}

¹*Department of Physics, Indian Institute of Technology (BHU), Varanasi, India 221005 and*

²*S. N. Bose National Centre for Basic Sciences,*

J D Block, Sector III, Salt Lake City, Kolkata 700106

(Dated: March 3, 2022)

Each agent in a collection of self-propelled particles (SPPs), in general can have different ability to influence their neighbours. We introduce a minimal model for a collection of SPPs interacting through a short-range alignment interaction, but the strength of the interaction is different for each particle, and it remains fixed with time. The interaction strength of each particle is obtained from a uniform distribution. For zero disorder, the model reduces to the clean system. We study the characteristics of the ordered steady-state and kinetics of the system for different strengths of the disorder. We find that the presence of disorder does not destroy the usual long-range ordering present in the clean system. Moreover, to our surprise, the density clustering is enhanced in the presence of disorder. The disorder introduces the formation of random network of different interaction strengths which leads to the slower dynamics of the particle, hence, enhances the cohesion among the particles. Furthermore, we note that kinetics to the ordered state remains unaffected due to the bond-disorder. The correlation length for the ordered domains and size of the particle density clusters grow with time, with the dynamic growth exponents $z_o \sim 2$ and $z_\rho \sim 4$, respectively.

I. INTRODUCTION

Collective behaviour of a large number of self-propelled particles (SPPs) or “flocking” is ubiquitous. Examples of such systems range from a few micrometres e.g., actin and tubulin filaments, molecular motors [1, 2], unicellular organisms such as amoebae and bacteria [3], to several metres e.g., bird flock [4], fish school [5] and human crowd [6] *etc.* Interestingly, these systems show a collective motion on a scale much larger than the each individuals, hence, long-range ordering (LRO) is observed even in two dimensions. A minimal model to understand the basic features of the collective behavior of self-propelled polar particles or “polar flock” was introduced in 1995 by T. Vicsek *et al.* [7]. In the last three decades, many variants of the Vicsek model are studied to understand various features of different model systems [9–12].

These studies, mainly consider the collection of SPPs in a homogeneous system or medium. Recently there is growing interest to understand the effects and advantages of different kinds of inhomogeneities which is omnipresent in nature. Many recent studies show that the inhomogeneity can destroy the LRO present in the system [13–21] whereas some special kinds of inhomogeneities can enhance the ordering [22, 23]. Therefore, the inhomogeneity can be useful for many practical applications e.g., crowd control and faster evacuation *etc.*[24–28].

In the Vicsek model, each individual interacts through a short-range alignment interaction and the interaction strength is same for all the particles. But in natural systems, each particle can have the different ability

to influence its neighbors, but not much attention has been paid to understand the effects of different interaction strengths in a polar flock. A recent study by William *et al.*, show that the varying interaction strength of the SPPs results to maximum entropy and hence more information transfer among the particles [35].

In this work, we introduce a collection of polar SPPs with *bond-disorder*. Each particle interact through a short range alignment interaction with varying interaction strength. The strength of interaction for each particle is different and obtained from a uniform distribution between $[1 - \epsilon/2 : 1 + \epsilon/2]$, ϵ is the strength of bond-disorder. For *zero*-disorder, model represents the clean polar flock with constant interaction strengths for all the particles, as for the Vicsek model [7]. The equilibrium analogue of the model is the XY-model with bond-disorder [36, 37]. Our focus is to understand the effects of the bond-disorder on the true long-range ordered state in the clean system [7, 8]. Furthermore, we have characterised the effects of the bond-disorder on the ordering kinetics of the polar flock.

We note that the presence of the disorder does not destroy the LRO present in the clean system. However, the disorder affects the density clustering and results in more *cohesive* flocking. Furthermore, we also studied the ordering kinetics of the orientation and the density field. When the system is quenched from the isotropic to the ordered steady state, both the orientation and the density field, coarsens with time. The size of the ordered high density domains grow with time, with an effective growth exponent for the orientation, $z_o \simeq 2$ (same as for non-conserved model A [39, 40] and the density $z_\rho \simeq 4$ (as found for conserved field in active systems)[41, 42]).

* jayps.rs.phy16@itbhu.ac.in

† sudipta.pattanayak@bose.res.in

‡ smishra.phy@iitbhu.ac.in

Rest of the paper is organised as follows. In Sec.II we discuss the model and simulation details. In Sec.III,

the results from numerical simulations are discussed. In Sec.IV, we conclude the paper with summary and discussion of the results. Appendix A, include the details of linearised hydrodynamic approach to calculate the local density fluctuation in the system.

II. MODEL

We consider a collection of N polar self-propelled particles (SPPs) moving on a two-dimensional substrate. SPPs interact through a short-range alignment interaction within a small interaction radius R_I [7, 9, 10]. Moreover, the strength of interaction of each SPP with its neighbors is *different*, unlike the Vicsek model [7] of uniform interaction strength. Furthermore, we also introduce a soft binary repulsive force \mathbf{f}_{ij} to consider the volume exclusion among the particles. Each SPP is defined by its position \mathbf{r}_i and orientation θ_i , and it moves along its direction vector $\mathbf{n}_i(t) = (\cos(\theta_i(t)), \sin(\theta_i(t)))$ with a fixed speed v_0 . The two update equations for the position $\mathbf{r}_i(t)$ and the direction vector $\mathbf{n}_i(t)$ are given by,

$$\mathbf{r}_i(t + \Delta t) = \mathbf{r}_i(t) + v_0 \mathbf{n}_i(t) \Delta t \quad (1)$$

$$\mathbf{n}_i(t + \Delta t) = \frac{\sum_{j \in R_I} J_j \mathbf{n}_j(t) + \beta \sum_{j \in R} \mathbf{f}_{ij} + \eta N_i(t) \xi_i(t)}{w_i(t)} \quad (2)$$

$$\mathbf{f}_{ij} = \left(\exp[1 - (\frac{r_{ij}}{R})^\gamma] - 1 \right) \mathbf{e}_{ij}. \quad (3)$$

$\mathbf{f}_{ij} \neq 0$ if $r_{ij} < R$, and $\mathbf{f}_{ij} = 0$ if $r_{ij} \geq R$, where $R = R_I/10$ is the typical size of the particles. $r_{ij} = |\mathbf{r}_j - \mathbf{r}_i|$, $\mathbf{e}_{ij} = \frac{\mathbf{r}_{ij}}{r_{ij}}$ and the exponent $\gamma = 0.25$ is kept fixed.

The first equation represent the motion of the particle due to its self-propelled nature, along the direction vector $\mathbf{n}(t)$ with fixed speed v_0 . $\Delta t = 1.0$ is the unit time step. The first term in Eq.2 represents the short-range alignment interaction of the i^{th} particle with its neighbors within the interaction radius (R_I), and J_j is the interaction strength of the j^{th} neighbor. The probability distribution of the interaction strength J , $P(J)$, is obtained from a uniform distribution of range $[1 - \frac{\epsilon}{2} : 1 + \frac{\epsilon}{2}]$ [37], where ϵ measures the degree of disorder. $\epsilon = 0$ corresponds to the uniform interaction strength ($J_i = 1$ for all the particles) like the Vicsek model [7] whereas $\epsilon = 2$ corresponds to the maximum disorder in the system. The second term indicates the soft-repulsive force due to the finite size of the particles and β , the strength of the force is kept fixed to 0.01. Furthermore, the third term in the Eq.2 denotes the vector noise which measures the error made by the particle during following its neighbors. $\xi_i(t)$ is a random unit vector, where $N_i(t)$ denotes the number of neighbors within the interaction radius of the i^{th} particle at time t . η represents the strength of the noise and can vary from 0 to 1. $w_i(t)$ is the normalisation factor, which reduces the R. H. S. of the Eq.2 to

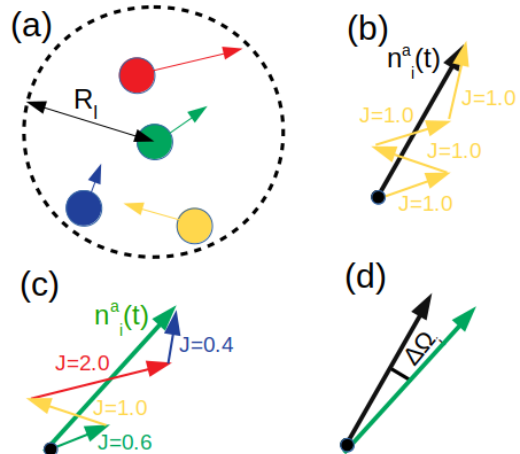


FIG. 1. (color online) (a) Cartoon picture of the model for RBDPF is shown. The dashed circle of radius R_I represents the interaction radius of the green tagged particle (at the centre). The neighbors of the tagged particle are shown by various colors. Small circles around the particles represent the approximate size of particles (radius R). The arrows of different lengths indicate the interaction strength J 's of the respective particles. (b) and (c) show the cartoon of the resultant direction of the tagged particle due to the alignment interaction with its neighbors for the constant strength (the clean polar flock) and the varying (RBDPF) interaction strength model, respectively. Bold black and green arrow represent the resultant direction \mathbf{n}_i^a (due to alignment interaction) of the tagged particle in (b) and (c), respectively. (d) The relative difference in the resultant direction $\Delta\Omega_i$ of the tagged particle for the clean and the RBDPF is shown.

a unit vector.

The cartoon picture of the model is shown in Fig.1 (a). The resultant direction vectors $\mathbf{n}_i^a(t)$ (due to alignment interaction) of the i^{th} particle with its neighbors for the clean ($\epsilon = 0$) and the disorder ($\epsilon = 2.0$) system are shown in Fig.1(b) and (c), respectively. In Fig.1(d), $\Delta\Omega_i$ denotes the difference in the resultant vector shown in Fig. 1(b) and (c). For zero self-propulsion speed model reduces to equilibrium random bond XY-model, hence we name the model as random bond disorder in polar flock (RBDPF). However, for $\epsilon = 0$, the model reduces to the clean polar flock. We numerically update the Eqs.1 and 2 for all SPPs sequentially. One simulation step is counted after the update of Eqs.1 and 2 once for all the particles. Periodic boundary condition (PBC) is used for a system of size $L \times L$, and L is varied from 50 to 512 (N from 2500 to 262144). The number density of the system is defined as $\rho_N = \frac{N}{L \times L}$. We fix the density at $\rho_N = 1.0$ and self-propulsion speed $v_0 = 0.5$. The noise strength η is fixed at $\eta = 0.2$, such that the clean system is in the homogeneous ordered state and hence away from the the order-disorder phase transition [10]. We study the steady-state as well as the ordering kinetics of the orientation and density field for different strengths of the disorder ϵ . We considered time up to 10^4 to study the ordering kinetics and steady state results are obtained from time up to 10^6 and 20 independent realisations are

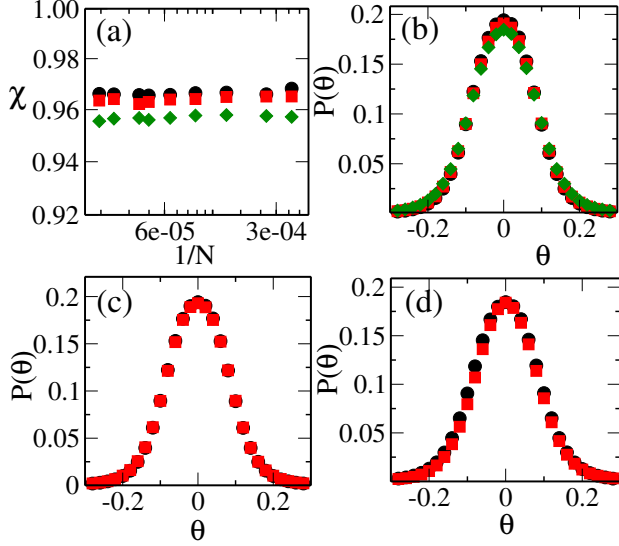


FIG. 2. (color online) (a) Plot of the mean value of global orientation order parameter χ vs. $1/N$ is shown for different ϵ in semi-log scale. (b) The PDF of the mean orientation fluctuation $P(\theta)$ is shown for different ϵ . $N = 62500$. The black circles, red squares, green diamonds represent data for $\epsilon = 0.0, 1.0$, and 2.0 , respectively. (c) and (d), plots of $P(\theta)$ vs. θ are shown for different system sizes for $\epsilon = 0.0$ and $\epsilon = 2.0$, respectively. The black circles and red squares denote $N = 40000$ and 62500 , respectively.

used for better statistics.

III. RESULTS

A. Steady-state behaviour

The orientation ordering in the system is characterised by the global orientation order parameter defined as, $\chi(t) = \frac{1}{N} |\sum_{i=1}^N \mathbf{n}_i(t)|$, $\chi(t)$ is zero for the disordered state and it is close to unity in the ordered state. The variation of mean value of $\chi(t)$, χ vs. $1/N$ for different ϵ is shown in Fig.2(a), where “mean” is obtained from the $\chi(t)$ in the steady state and 20 independent realisations. We note that χ is independent of system size for different strengths ϵ of the disorder. However, the magnitude of χ shows a small variation on increasing the strength ϵ of the disorder. Furthermore, the probability distribution function (PDF) of the orientation of the particles $P(\theta)$ is shown for different values of ϵ in Fig.2(b). The PDF widens with the increasing disorder strength ϵ , moreover, the change is small but it is consistent on increasing ϵ . To confirm the long-range ordering, we plot $P(\theta)$ for two different system sizes for $\epsilon = 0$ and 2 , in Fig.2(c) and (d), respectively. $P(\theta)$ distribution for different system sizes overlaps on each other for a particular ϵ . Therefore, the magnitude of the global ordering shows a small decay with increasing ϵ but the ordered steady-state remains long-range for all ϵ for RBDPF.

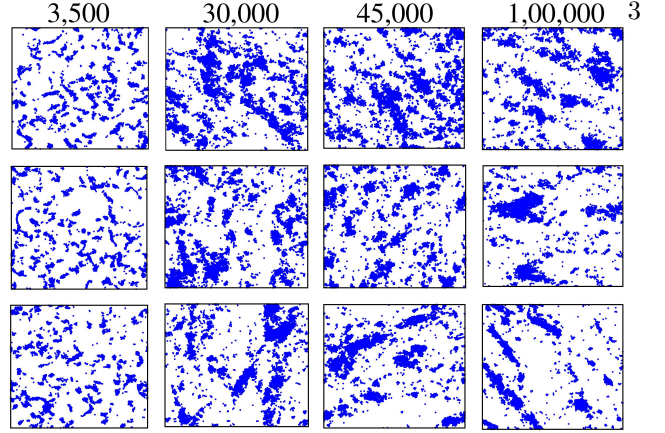


FIG. 3. (color online) (a) Real space snapshots of the particles' position for different ϵ are shown at different times t . $N = 10000$. Top to bottom panels are for $\epsilon = 0, 1$ and 2 , respectively.

Behaviour of the flock state

As discussed in previous paragraph, the disorder does not affect the usual long-range ordering in the system. Furthermore, we study the effect of the disorder on the clustering of particles in the steady-state. The snapshots of system for three different strengths of the disorder, $\epsilon = 0, 1$ and 2 at different times are shown in Fig.3. It is clear that the particles cluster more strongly for larger ϵ . To further characterise the density clustering, we calculate the probability distribution function (PDF) $P(n, \epsilon)$ of number of particles inside the interaction radius for different ϵ . $P(n, \epsilon)$ for different ϵ decay with an exponential tail, $P(n, \epsilon) \sim P_o(\epsilon) \exp(-n/n_c(\epsilon))$, as shown in Fig.4(a). The distribution flattens with the increasing strength of the disorder. Therefore, the particles are having more number of neighbors inside its interaction radius, i.e. more compact/dense clustering in the system. In the Fig.4(b), the plot of $P(n, \epsilon)/P_o(\epsilon)$ vs. $n/n_c(\epsilon)$ is shown for different ϵ . The scaling of the PDF confirms that the clusters are statistically identical for different strengths ϵ of the disorder. To further understand the density clustering, we calculate the local density fluctuation, $\delta\phi(\epsilon) = \sqrt{\frac{1}{L^2} \sum_{j=1}^{L^2} (\phi_j(\epsilon))^2 - (\frac{1}{L^2} \sum_{j=1}^{L^2} \phi_j(\epsilon))^2}$, for different ϵ . To calculate $\delta\phi(\epsilon)$, we divide the full $L \times L$ system into L^2 number of unit sized sub-cells. $\phi_j(\epsilon)$ is the number of particles in the j^{th} unit sized sub-cell and $\delta\phi(\epsilon)$ is the measure of the local density fluctuations in the system for a given ϵ . Furthermore, we define the relative density phase separation by $\Delta\Phi(\epsilon) = \delta\phi(\epsilon) - \delta\phi(0)$, where $\delta\phi(0)$ is the local density fluctuation for the clean system, $\epsilon = 0$. The plot of $\Delta\Phi(\epsilon)$ vs. ϵ is shown in Fig.4(c). We note that the density clustering increases with ϵ . We also calculate the magnitude of the density fluctuation using linearised hydrodynamic equations of motion for the coarse-grained density and the orientation fields of the system. The dashed line in Fig.4(c) is obtained from the linearised hydrodynamics and it is

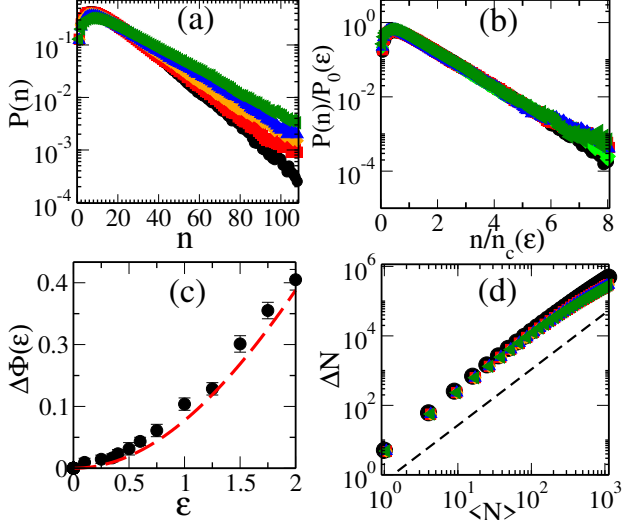


FIG. 4. (color online) (a) The plot of the PDF $P(n, \epsilon)$ vs. the mean number of the particles n inside the interaction radius for different ϵ are shown in semi-log y-scale. (b) The plot of $P(n, \epsilon)/P_0(\epsilon)$ vs. n/n_c is shown. The black circles, red squares, orange diamonds, blue triangles up, and green triangles left represent $\epsilon = 0.0, 0.5, 1.0, 1.5,$ and 2.0 , respectively. $N = 62500$. (c) Variation of $\Delta\Phi(\epsilon)$ with ϵ is shown. The filled black circles are the numerical data points with error bars, $N = 62500$. The red dashed line indicates the $\Delta\Phi(\epsilon)$ obtained from the analytical calculations, as shown in the Appendix.A Eq. A22. (d) Plot of the mean density fluctuation ($\Delta\mathcal{N}$) vs. $\langle\mathcal{N}\rangle$ is shown in log – log scale. $N = 62500$. The dashed line has slope = 1.6.

consistent with the numerical data. The details of the hydrodynamic calculation is given in the Appendix A. Therefore, the bond-disorder which intuitively have a tendency to disturb the ordering in the corresponding equilibrium system [37, 38], enhances the density clustering in RBDPF. Hence, the disorder introduces more *cohesion* among the SPPs.

Although the disorder affects the local density clustering but the global number fluctuation in different sub-systems, $\Delta\mathcal{N} = \sqrt{\langle\mathcal{N}^2\rangle - \langle\mathcal{N}\rangle^2}$, remains unaffected in the presence of the disorder and shows the usual Giant number fluctuation (GNF). We show the plot of $\Delta\mathcal{N}$ vs. the mean number of particles in the sub-system $\langle\mathcal{N}\rangle$ for different ϵ in Fig.4 (d). We note that $\Delta\mathcal{N} \simeq \langle\mathcal{N}\rangle^{1.6}$, and it matches well with the previous studies of polar self-propelled particles interact through the Vicsek type interaction [9, 10, 43].

Distribution of particles in flock

In the previous section, we note that the bond-disorder introduces more cohesion among the SPPs. To understand this mechanism of cohesion for large disorder, we analyse a cluster and study the distribution of particles inside it, as shown in Fig.5. The snapshot of particles' position in the system is shown in Fig.5(a). The dif-

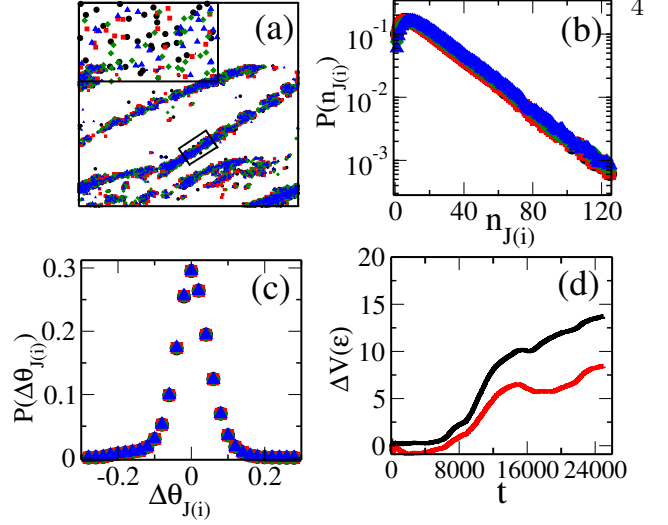


FIG. 5. (color online) (a) Snapshot of the particles' position in the steady-state for disorder strength $\epsilon = 2.0$ is shown. $N = 10000$. The black circles, red squares, green diamonds, and blue triangles denote $0 \leq J < 0.5$, $0.5 \leq J < 1.0$, $1.0 \leq J < 1.5$, and $1.5 \leq J \leq 2.0$, respectively. *Inset*: The zoomed picture of the box in the main figure is shown. All the particles in the *inset* belong to a single cluster. (b-c) Plot of the PDFs $P(n_{J(i)})$ and $P(\theta_{J(i)})$ are shown, respectively. $N = 62500$. Symbols have same meaning as in (a). (d) The percentage difference in the effective mean speed $\Delta v(\epsilon)$ of a tag particle vs. time t is shown. The black and red bold lines represent $\epsilon = 1.0$ and $\epsilon = 2.0$, respectively. $N = 10000$.

ferent ranges of the interaction strength for particles is shown by different colors. The four colors are obtained by dividing the full range of $J \in [0, 2]$ in four parts $J(1) \in [0 : 0.5]$, $J(2) \in [0.5, 1.0]$, $J(3) \in [1.0 : 1.5]$ and $J(4) \in [1.5 : 2.0]$ for $\epsilon = 2$. The zoomed picture of one cluster is shown in Fig.5(a) (*inset*), which shows that the particles of different interaction strengths are distributed homogeneously inside a cluster. Furthermore, we calculate the PDF, $P(n_{J(i)})$ of the number of particles $n_{J(i)}$ of the different interaction ranges, inside the interaction radius for $\epsilon = 2$. The plot of $P(n_{J(i)})$ is shown in Fig.5(b). The near identical $P(n_{J(i)})$ for each range of $J(i)$, where $i = 1, 2, 3, 4$, confirms that particles are distributed homogeneously in the system. We also plot the particles orientation distribution $P(\theta_{J(i)})$ for the four different ranges of $J(i)$. The local orientation distribution of the particles of different ranges $P(\theta_{J(i)})$ remain unchanged, as shown in the Fig.5(c). The distribution of particles and their corresponding orientation distributions are homogeneous inside a cluster, hence, the network of particle is homogeneous for RBDPF. Therefore, a moving particle experiences a random network of interaction strengths during its motion. Now we measure the effect of such random network on the particle motion. We calculate the effective mean speed, $v(\epsilon)$ of a tag particle for different disorder. We find that the larger the disorder slows the effective speed. Hence for a given tag particle, $v(\epsilon)$ decreases with increasing

ϵ . To compare the effective speed for finite disorder we calculate the percentage change in $v(\epsilon)$ for any finite disorder with respect to the clean system $v(0)$. We define $\Delta v(\epsilon) = \left| \frac{v(\epsilon) - v(0)}{v(0)} \right| \%$, and in Fig. 5(d) we plot $\Delta v(\epsilon)$ with time t for two different ϵ . Clearly $\Delta v(\epsilon)$ increases with increasing time and larger for larger disorder. Hence larger the disorder, slower will be the speed of the tag particle. Hence we conclude that disorder leads to the formation of random network of interaction strengths of its neighbours, which results in slower dynamics of the particle. Hence responsible for the strong clustering for larger disorder.

B. Dynamical Behaviour

Ordering kinetics to the steady state

In previous sections, we have discussed the steady-state properties of the ordered state. Furthermore, we study the effects of the bond-disorder on the ordering kinetics when the system is quenched from a random disordered state to an ordered steady-state. Kinetics of the orientation ordering and the density clustering are characterised by calculating the two-point orientation correlation function $C(r, t) = \left\langle \frac{\sum_{ij} \mathbf{n}_i(r_0, t) \cdot \mathbf{n}_j(r_0 + r, t)}{\sum_{ij} |\mathbf{n}_i(r_0, t)| \cdot |\mathbf{n}_j(r_0 + r, t)|} \right\rangle$ and the size of the largest density cluster $m(t)$, respectively. The $\langle \dots \rangle$ means average over many r_0 's and 10 independent realisations. We note that $C(r, t)$ grows with time for all disorder strengths ϵ and its growth is characterised by calculating the size of the growing domain $L_o(t)$ which is obtained from the first zero crossing of $C(r, t)$. The plot of $L_o(t)$ vs. time t for the clean system $\epsilon = 0$ and for the RBDPF ($\epsilon = 1, 2$) is shown in Fig.6(a). We note that the disorder has no effect on the kinetics of growing domains. Moreover, the size of domains varies as, $L_o(t) \simeq t^{1/z_o}$ with $z_o \sim 2$ for all disorder strengths. We also calculate the growth of the density cluster. The size of the largest cluster $m(t)$ is calculated using the cluster counting algorithm [44]. The plot of $m(t)$ vs. time t for the clean system and the RBDPF, $\epsilon = 1, 2$ is shown in Fig. 6(b). For all cases, $m(t)$ grows with time as t^α with $\alpha \sim 0.5$. Hence, the length of the density cluster $L_\rho(t) \simeq \sqrt{m(t)} \sim t^{1/z_\rho}$ and $z_\rho \sim 4$, which is similar to the asymptotic growth exponent for the conserved field in the active model B [41, 42].

IV. DISCUSSION

We introduced a minimal model of a collection of self-propelled particles with bond-disorder. Each particle has a different ability (interaction strength) to influence its neighbours. The varying interaction strength is obtained from a uniform distribution and it can be varied from $[1 - \epsilon/2 : 1 + \epsilon/2]$, where ϵ is the disorder strength. For $\epsilon = 0$, the model reduces to the constant interaction

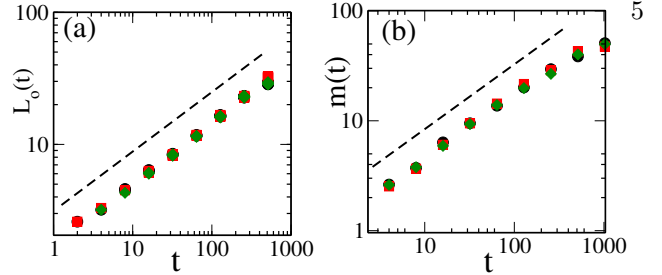


FIG. 6. (color online) (a) Plot of the correlation length of the orientation field $L_o(t)$ with time t is shown on log – log scale. The dashed line represents the slope 0.5. $N = 262144$. (b) Plot of mass of the largest cluster $m(t)$ with time t is shown in log – log scale. $N = 40000$. The dashed line represents the slope 0.5. The black filled circles, red filled squares, and green filled diamonds represent $\epsilon = 0, 1, 0$ and $2, 0$, respectively.

strength model or the Vicsek-like model [7]. The equilibrium analogue of the present model is random bond XY model. We studied the characteristics of the ordered steady-state for different strength of the disorder. The bond disorder does not affect the usual LRO present in the clean polar flock. To our surprise, the bond disorder leads to more cohesive flock, hence, more inhomogeneous or dense clusters. This phenomenon is due to the slower dynamics of particles moving in the random network of different interaction strengths. Although the disorder affects the local density inhomogeneity but the global density fluctuation remains unaffected and the system shows the usual giant number fluctuation (GNF). Furthermore, we also studied the effect of the bond disorder on the ordering kinetics of the orientation and the density field. The orientation field coarsens with time with the dynamics growth exponent $z_o \sim 2$ whereas the growth exponent for the density field $z_\rho \sim 4$ and coarsening for both the field remains unaffected in the presence bond-disorder as opposed to what is observed in the corresponding equilibrium model [37, 38]. Hence, our study introduces the effect of the bond disorder in polar flock and shows many interesting features which is in general not present in corresponding equilibrium system with bond-disorder [37, 38]. It also opens a new direction to understand the effect of bond-disorder in polar flock, which is very much present in many natural systems.

Appendix A: Linearised study of hydrodynamic equations of motion

We begin by defining the local density field for the particles. such that

$$\rho(\mathbf{r}, t) = \sum_{i=1}^N \delta(\mathbf{r} - \mathbf{r}_i) \quad (\text{A1})$$

where \mathbf{r}_i and N , are the position vector of the i^{th} particle and total number of particles respectively. Similarly we

define the local polarization field as

$$\mathbf{P}(\mathbf{r}, t) = \frac{\sum_{i=1}^N \mathbf{n}_i(t) \delta(\mathbf{r} - \mathbf{r}_i)}{\rho(\mathbf{r}, t)}, \quad (\text{A2})$$

With the help of the local fields defined in Eq.A1 and A2 and the two update equations 1 and 2, we can write the coarse-grained hydrodynamic equations of the motion for local density and polarisation.

$$\partial_t \rho = -v_0 \nabla \cdot (\mathbf{P} \rho) + D_\rho \nabla^2 \rho + \mathbf{\Delta} \cdot \mathbf{f}_\rho \quad (\text{A3})$$

$$\partial_t \mathbf{P} = (\alpha_1(\rho, \epsilon) - \alpha_2 \mathbf{P} \cdot \mathbf{P}) \mathbf{P} - \frac{v_1}{2\rho_0} \nabla(\rho) + \lambda(\mathbf{P} \cdot \nabla) \mathbf{P} + D_\rho \nabla^2 \rho \quad (\text{A4})$$

The above two equations are of the same form as given in [8], we introduced a density and disorder dependent $\alpha_1(\rho, \epsilon)$. The form for $\alpha_1(\rho, \epsilon)$ is obtained from the derivation of hydrodynamic equations of motion using the two update equations 1 and 2. We find that $\alpha_1(\rho, \epsilon) = \alpha_0(\rho(\frac{1+\epsilon^2/12}{1-\epsilon^2/84}) - \eta^2)$, where α_0 is a constant of $\mathcal{O}(1)$. We assume all other terms independent of disorder for simplicity. The density Eq. A3 is a continuity equation, with a flux controlled by two terms: $-v_0 \nabla \cdot (\mathbf{P} \rho)$ describing convection due to self-propulsion speed, $v_0 \mathbf{P}$, and a diffusion term $D_\rho \nabla^2 \rho$ that drives the density to a homogeneous state. In the R.H.S of Eq. A4, first term make sure a mean field transition from an isotropic ($\mathbf{P} = 0$) to broken symmetry state $\mathbf{P} = \sqrt{\frac{\alpha_1(\rho_0, \epsilon)}{\alpha_2}} \hat{\mathbf{x}}$ (the direction of broken symmetry is chosen along x -axis). The second term is the convection in polarisation due to density gradient, third term is non-linear term present in the model and the fourth term is diffusion in polarisation equation. The last terms in A3 is conservative noise with \mathbf{f}_ρ , the Gaussian random forces with mean zero and variance $\mathbf{\Delta}_\rho$. Now we perturb the system about the homogeneous steady state solution of Eqs. A3 and A4 and write $\rho(\mathbf{r}, t) = \rho_0 + \delta\rho$ and $\mathbf{P}(\mathbf{r}, t) = (p_0 + \delta p_\parallel) \hat{\mathbf{x}} + (\delta p_\perp) \hat{\mathbf{y}}$, where $p_0 = \sqrt{\frac{\alpha_1(\rho_0, \epsilon)}{\alpha_2}}$. Now we write the linearised hydrodynamic equations for small perturbations in three fields $\delta\rho$, δp_\parallel and δp_\perp , where p_\parallel and p_\perp is the direction of broken symmetry and perpendicular to it respectively. We first write the equation for δp_\parallel

$$\begin{aligned} \partial_t \delta p_\parallel &= (\alpha_1(\rho_0, \epsilon) + \alpha_1'(\rho_0) \delta\rho)(p_0 + \delta p_\parallel) - \frac{v_1}{2\rho_0} \delta_x \rho \\ &\quad - \alpha_2(p_0^2 + 2p_0 \delta p_\parallel)(p_0 + \delta p_\parallel) + \lambda(p_0 \partial_x) \delta p_\parallel + D_\rho \nabla^2 \delta p_\parallel \end{aligned} \quad (\text{A5})$$

and

$$\partial_t \delta p_\perp = \lambda p_0 \partial_x \delta p_y + D_\rho \nabla^2 \delta p_y - \frac{v_1}{2\rho_0} \partial_y \delta \rho \quad (\text{A6})$$

and

$$\partial_t \delta \rho = -v_0(\partial_x(p_0 + \delta p_\parallel)(\rho_0 + \delta\rho) + \partial_y \delta p_y(\rho_0 + \delta\rho)) + D_\rho \nabla^2 \delta \rho + \nabla \cdot \mathbf{f}_\rho \quad (\text{A7})$$

where $\alpha_1' = \frac{\partial \alpha_1(\rho)}{\partial \rho}|_{\rho_0} = \alpha_0 \frac{(1+\epsilon^2/12)}{(1-\epsilon^2/84)}$, we ignore the higher order fluctuations in δp_\parallel and in the steady state solve for δp_\parallel

$$\delta p_\parallel = \frac{\alpha_1' p_0 - \frac{v_1}{2\rho_0} \partial_x \delta \rho}{2\alpha_1(\rho_0, \epsilon)} \quad (\text{A8})$$

Now we substitute for δp_\parallel from Eq. A8 in Eqs. A6 and A7 and write an effective dynamical equations for δp_\perp and $\delta \rho$

$$\partial_t \delta p_\perp = \lambda p_0 \partial_x \delta p_y + D_\rho \nabla^2 \delta p_y - \frac{v_1}{2\rho_0} \partial_y \delta \rho \quad (\text{A9})$$

$$\partial_t \delta \rho = v_0 p_0 V_x \partial_x \delta \rho + D_{\rho x} \partial_x^2 \delta \rho + D_\rho \partial_y^2 \delta \rho - v_0 \rho_0 \partial_y \delta p_\perp \quad (\text{A10})$$

where $V_x = (\frac{\rho_0 \alpha_1'}{2\alpha_1} + 1)$ and $D_{\rho x} = D_\rho + \frac{v_0 v_1}{4\alpha_1}$, where $\alpha_1 = \alpha_1(\rho_0, \epsilon)$. Now taking the Fourier transform $Y(\mathbf{r}, t) = \int d\mathbf{k} \exp(-i(\mathbf{k} \cdot \mathbf{r} + \omega t)) Y(\mathbf{k}, \omega)$ and writing the two equations A9 and A10 in matrix notation

$$M \begin{bmatrix} \delta \rho \\ \delta p_\perp \end{bmatrix} = \begin{bmatrix} \mathbf{i} \mathbf{q} \cdot \mathbf{f}_\rho \\ 0 \end{bmatrix} \quad (\text{A11})$$

where the coefficient matrix M can be written as

$$M = \begin{bmatrix} (-i\omega + iq_x v_0 p_0 V_x - D_{\rho x} q_x^2 - D_{\rho y} q_y^2) & (-v_0 \rho_0 i q_y \delta p_y) \\ (\frac{i v_1}{2 \rho_0} q_y \delta \rho) & (-i\omega - \lambda p_0 i q_x - D_{\rho} q^2) \end{bmatrix} \begin{bmatrix} \delta \rho \\ \delta p_{\perp} \end{bmatrix} \quad (\text{A12})$$

The Eq. A12 gives the two modes of the linearised hydrodynamics

$$\omega_{\pm} = C_{\pm}(\theta)q - i\Gamma_L \left[\frac{V_{\pm}(\theta)}{2C_2(\theta)} \right] - i\Gamma_{\rho} \left[\frac{V_{\pm}(\theta)}{2C_2(\theta)} \right] \quad (\text{A13})$$

where $C_{\pm}(\theta) = \frac{\gamma + v_0 V_x}{2} \cos \theta \pm C_2(\theta)$, $C_2(\theta) = \sqrt{\frac{(\gamma - v_0 V_x)^2 \cos^2 \theta}{4} + \rho_0 v_1 \sin^2 \theta}$, and $\gamma = -\lambda v_0$. Here θ is the angle between flock direction and propagation vector \mathbf{q} . $\Gamma_{\rho}(q) = D_{\rho} q_y^2 + D_{\rho x} q_x^2$, $\Gamma_L(q) = D_{\rho} q^2$ and $V_{\pm}(\theta) = C_2(\theta) \pm \frac{\gamma - v_0 V_x}{2} \cos \theta$. Here $\Gamma_{\rho}(q)$ and $\Gamma_L(q)$ are the wave vector dependent damping. Using Eq. A12 we get

$$\begin{bmatrix} \delta \rho \\ \delta p_{\perp} \end{bmatrix} = M^{-1} \begin{bmatrix} \mathbf{iq} \cdot \mathbf{f}_{\rho} \\ 0 \end{bmatrix} \quad (\text{A14})$$

Hence solution for fluctuation in ρ , $\delta \rho(q, \omega) = G_{\rho\rho}(q, \omega) \mathbf{iq} \cdot \mathbf{f}_{\rho}(\mathbf{q}, \omega) = G_{\rho\rho} \mathbf{iq} \cdot \Delta_{\rho}$. The density propagator $G_{\rho\rho}(q, \omega)$ can be written as

$$G_{\rho\rho}(q, \omega) = \frac{-i(\omega - \gamma q \cos \theta) + \Gamma_L(q)}{(\omega - C_+(\theta)q)(\omega - C_-(\theta)q) + i\omega(\Gamma_{\rho}(q) + \Gamma_L(q))(-iq \cos \theta \gamma \Gamma_{\rho}(q) + v_0 V_x \Gamma_L(q))} \quad (\text{A15})$$

Hence the two-point density-density correlation function $C_{\rho\rho} = \langle |\delta \rho(q, \omega)|^2 \rangle$ is

$$C_{\rho\rho} = \frac{(\omega - q\gamma \cos \theta)^2 (q^2 \Delta_{\rho})}{(\omega - C_+(\theta)q)^2 (\omega - C_-(\theta)q) + \omega(\Gamma_{\rho}(q) + \Gamma_L(q))(-q \cos \theta \gamma \Gamma_{\rho}(q) + v_0 V_x \Gamma_L(q))^2} \quad (\text{A16})$$

Now we calculate the density fluctuation $\langle |\delta \rho(\mathbf{q}, \omega)| \rangle$, and it can be obtained from

$$\sqrt{C_{\rho\rho}} = \left[\frac{(C_+(\theta)q - \gamma q \cos \theta)q \sqrt{\Delta_{\rho}}}{C_+(\theta)q(\Gamma_{\rho} + \Gamma_L) - q \cos \theta (\gamma \Gamma_{\rho} + v_0 V_x \Gamma_L)} \right] + \left[\frac{(C_+(\theta)q - \gamma q \cos \theta)q \sqrt{\Delta_{\rho}}}{C_-(\theta)q(\Gamma_{\rho} + \Gamma_L) - q \cos \theta (\gamma \Gamma_{\rho} + v_0 V_x \Gamma_L)} \right] \quad (\text{A17})$$

Hence the fluctuation in local density in the steady-state

$$\langle |\delta \rho(q)| \rangle = \frac{(C_+(\theta) - \gamma \cos \theta)q \sqrt{\Delta_{\rho}}}{(C_+(\theta)(D_{\rho} \sin^2 \theta + D_{\rho x} \cos^2 \theta) - \cos \theta ((\gamma D_{\rho} \sin^2 \theta + D_{\rho x} \cos^2 \theta) + v_0 V_x D_L))} + \frac{(C_-(\theta) - \gamma \cos \theta)q \sqrt{\Delta_{\rho}}}{(C_-(\theta)(D_{\rho} \sin^2 \theta + D_{\rho x} \cos^2 \theta) - \cos \theta ((\gamma D_{\rho} \sin^2 \theta + D_{\rho x} \cos^2 \theta) + v_0 V_x D_L))} \quad (\text{A18})$$

More simpler form of Eq. A18 can be written as

$$\langle |\delta \rho(q)| \rangle = \sqrt{\Delta_{\rho}} \left[\frac{(C_-(\theta) - \gamma)(\gamma_+(\theta) D_{\rho x} - A) + (C_+(\theta) - \gamma)(C_-(\theta) D_{\rho x} - A)}{(c_+(\theta) D_{\rho x} - A)(c_-(\theta) D_{\rho x} - A)} \right] \quad (\text{A19})$$

Here $A = \gamma D_{\rho x} + v_0 V_x D_L$, $C_+ + C_- = \frac{\gamma + v_0 V_x}{2}$, $C_+ C_- = \gamma v_0 V_x$. Substituting these values into Eq. A19 and after simplification it gives

$$\langle |\delta \rho| \rangle = \frac{\frac{\gamma v_0 V_x (D_{\rho x} + 3D_L)}{2} - \frac{v_0^2 V_x^2 D_L}{2}}{\gamma v_0 V_x D_L D_{\rho x} + D_L V_x^2 v_0^2 (D_L - D_{\rho x})} \quad (\text{A20})$$

where $V_x = 1 + \rho_0 \delta(\epsilon) \Rightarrow V_x = 1 + \delta(\epsilon)$, $\delta(\epsilon) = \frac{(1 - \frac{\epsilon^2}{84})}{(1 + \frac{\epsilon^2}{12})} \simeq 1 - 0.1\epsilon^2$. After simplification equation A20 reduced to

$$\langle |\delta \rho| \rangle = \frac{[(3 + \frac{D_{\rho x}}{D_p}) - 2(1 + \delta(\epsilon))]}{\frac{D_{\rho x}}{D_p} - 2(\frac{D_{\rho x}}{D_p} - 1)(1 + \delta(\epsilon))} \quad (\text{A21})$$

Substituting the value of $\delta(\epsilon)$ and $\frac{D_{\rho x}}{D_p} \sim 1$ in equation A21 and after simplification we get

$$\langle |\delta \rho| \rangle = \frac{(0.1 + 0.1\epsilon^2)}{0.2 + 0.02\epsilon^2} \quad (\text{A22})$$

-
- [1] F. Nédélec, Ph.D. thesis, University Paris **11**, 1998; F. Nédélec, T. Surrey, A. C. Maggs, and S. Leibler, *Nature (London)* **389**, 305 (1997).
- [2] H. Yokota (private communication); Y. Harada, A. Noguchi, A. Kishino, and T. Yanagida, *Nature (London)* **326**, 805 (1987); Y. Toyoshima et al., *Nature (London)* **328**, 536 (1987); S. J. Kron and J. A. Spudich, *Proc. Natl. Acad. Sci. U.S.A.* **83**, 6272 (1986).
- [3] J. T. Bonner, *Proc. Natl. Acad. Sci. U.S.A.* **95**, 9355 (1998); M. T. Laub and W. F. Loomis, *Mol. Biol. Cell* **9**, 3521 (1998).
- [4] D. Chen, Y. Wang, G. Wu, M. Kang, Y. Sun, and W. Yu, *Chaos* **29**, 113118 (2019).
- [5] *Three Dimensional Animals Groups*, edited by J. K. Parrish and W. M. Hamner (Cambridge University Press, Cambridge, England, 1997).
- [6] D. Helbing, I. Farkas, and T. Vicsek, *Nature (London)* **407**, 487 (2000).
- [7] T. Vicsek, A. Czirók, E. Ben-Jacob, I. Cohen, and O. Shochet, *Phys. Rev. Lett.* **75**, 1226 (1995).
- [8] J. Toner and Y. Tu, *Phys. Rev. E* **58**, 4828 (1998).
- [9] G. Grégoire and H. Chaté, *Phys. Rev. Lett.* **92**, 025702 (2004).
- [10] H. Chaté, F. Ginelli, Guillaume Grégoire, and F. Raynaud, *Phys. Rev. E* **77**, 046113 (2008).
- [11] S. Pattanayak and S. Mishra, *Journal of Physics Communications*, **2**, 045007 (2018).
- [12] M. Romensky, V. Lobaskin, and T. Ihle, *Phys. Rev. E* **90**, 063315 (2014).
- [13] A. Morin, N. Desreumaux, J. Caussin, and D. Bartolo, *Nature Physics* **13**, 6367 (2017).
- [14] O. Chepizhko, E. G. Altmann, and F. Peruani, *Phys. Rev. Lett.* **110**, 238101 (2013).
- [15] D. Yllanes, M. Leoni, and M. C. Marchetti, *New Journal of Physics* **19**, 103026 (2017).
- [16] D. A. Quint and A. Gopinathan, *Phys. Biol.* **12**, 046008 (2015).
- [17] C. Sándor, A. Libál, C. Reichhardt, and C. J. Olson Reichhardt, *Phys. Rev. E* **95**, 032606 (2017).
- [18] C. J. O. Reichhardt and C. Reichhardt, *Nat. Phys.* **13**, 10 (2017).
- [19] R. Das, M. Kumar, and S. Mishra, *Phys. R. E.* **98**, 060602(R) (2018).
- [20] J. Toner, N. Guttenberg, and Y. Tu, *Phys. Rev. E* **98**, 062604 (2018).
- [21] J. Toner, N. Guttenberg, and Y. Tu, *Phys. Rev. Lett.* **121**, 248002 (2018).
- [22] R. Das, M. Kumar, and S. Mishra, *Phys. Rev. E* **101**, 012607 (2020).
- [23] S. Pattanayak, M. Kumar, and S. Mishra, arXiv:2001.06584 (2020).
- [24] Guo-yuan Wang, Fan-yu Wu, You-liang Si, Q. Zeng, and P. Lin, *Procedia Engineering* **211**, 699 (2018).
- [25] G. A. Frank and C. O. Dorso, *Physica A (Amsterdam, Neth.)* **390**, 2135 (2011).
- [26] A. Garcimartn, D. R. Parisi, J. M. Pastor, C. Martn-Gómez, and I. Zuriguel, *J. Stat. Mech.* **4**, 043402 (2016).
- [27] I. Zuriguel, J. Olivares, J. M. Pastor, C. Martín-Gómez, L. M. Ferrer, J. J. Ramos, and A. Garcimartn, *Phys. Rev. E* **94**, 032302 (2016).
- [28] I. Zuriguel, A. Janda, A. Garcimartn, C. Lozano, R. Arévalo, and D. Maza *Phys. Rev. Lett.* **107**, 278001 (2011).
- [29] V. L. Berezinskii, *JETP* **32**, 493 (1971).
- [30] J. M. Kosterlitz and D. J. Thouless, *J. Phys. C* **6**, 1181 (1973).
- [31] J. M. Kosterlitz, *J. Phys. C* **7**, 1046 (1974).
- [32] S. Puri and C. Roland, *Phys. Lett. A* **151**, 500 (1990).
- [33] S. Puri, *Phys. Lett. A* **164**, 211 (1992).
- [34] S. Puri, D. Chowdhury, and N. Parekh, *J. Phys. A* **24**, L1087 (1991).
- [35] W. Bialek, A. Cavagna, I. Giardina, T. Mora, E. Silvestri, M. Viale, and A. M. Walczak, *PNAS* **109**, 4786 (2012).
- [36] Vik. S. Dotsenko and M. V. FeTgel'man, *Zh. Eksp. Teor. Fiz.* **83**, 345 (1982).
- [37] M. Kumar, S. Chatterjee, R. Paul, and S. Puri, *Phys. Rev. E* **96**, 042127 (2017).
- [38] D. J. Bishop and J. D. Reppy, *Phys. Rev. Lett.* **40**, 1727(1978).
- [39] A. J. Bray, *Advances in Physics* **43**, 357 (1994).
- [40] S. Puri, and V. Wadhawan, *Kinetics of Phase Transitions*, CRC press (2009).
- [41] R. Wittkowski, A. Tiribocchi, J. Stenhammar, R. J. Allen, D. Marenduzzo, and M. E. Cates, *Nature Communications* **5**, 4351 (2014).
- [42] S. Pattanayak, S. Mishra, and S. Puri, to be submitted.
- [43] B. Bhattacharjee, S. Mishra, S.S. Manna, *Phys. Rev. E.* **92**, 062134 (2015).
- [44] C. P. Beatrice, R. M. C. de Almeida, and L. G. Brunnet, *Phys. Rev. E.* **95**, 032402 (2017).